RESEARCH PAPER

Evaluation of solidification cracking of Ni-based alloy dissimilar welds based on Trans-Varestraint test

Georgia Effgen Santos[1] · Émerson Mendonça Miná[1] · Doroteu Afonso Coelho Pequeno[1] ·
Hélio Cordeiro de Miranda[1] · Cleiton Carvalho Silva[1]

Abstract

This study aims to evaluate the weldability of dissimilar welds with the Inconel 625 and the Hastelloy C-276 nickel-based alloys deposited on ASTM A36 and AISI 1045 carbon steel plates. The welds were carried out by the GMAW process and evaluated by the Trans-Varestraint test. The test results were statistically evaluated, and Fusion Zone solidification processes were simulated in JMatPro software using several dilution levels. The analysis of variance (ANOVA) test results showed that the two different base metals did not affect the weldability of Inconel 625. However, the Hastelloy C-276 alloy showed a significant drop in weldability with the AISI 1045 steel compared to the ASTM A36. The results of the Hastelloy C-276 as the filler metal and the AISI 1045 steel as the base metal showed greater susceptibility to solidification cracking than all the other pairs tested, according to the Trans-Varestraint test. Moreover, the ANOVA test results indicated that the different heat input levels did not influence the sets' weldability; this was probably because there was only a tiny variation in the dilution levels. The solidification process simulation indicates that higher dilution levels promote the precipitation of a larger secondary phase fraction.

1 Introduction

Dissimilar welding is a procedure in which two or more materials are melted and solidified together for different purposes. This procedure can result in a weld metal with specific properties or it can be used to assure the continuation of the joint properties, and it is frequently used to manufacture and repair pipes and equipment in industries [1–4]. Among the advanced materials most used in dissimilar welding are the Ni-based alloys due to their high corrosion resistance and a great combination of strength and toughness for a wide range of temperatures [5–10]. However, due to their high cost, these alloys are impracticable for large structures and equipment.

One alternative has been the use of these alloys mentioned above as weld claddings. Weld cladding is defined by Silva [11] as the deposition of one or more layers of a corrosion-resistant alloy (CRA) on a base metal to improve a desirable property, such as corrosion-resistant that is not inherent to the base metal. These coatings can be deposited by various manufacturing processes such as shielded metal arc welding (SMAW) 12, 13, gas tungsten arc welding (GTAW) [14–17], gas metal arc welding (GMAW) [18–21], plasma transferred arc welding (PTA) [22–24], electro slag welding (ESW) [25–28], laser cladding [29–32], or microwave cladding [33].

Dupont et al. [34], in a review of welding materials for the energy industry, dedicated a special section addressed to weld overlays, highlighting their scientific and technological importance. Iannuzzi et al. [35] pointed out that welding and cladding of dissimilar materials are recurrent in the subsea oil and gas industry. Significant investments have been made to develop and optimize the welding procedures of special materials for joining and cladding [36–39].

Recent investigations regarding Ni-based alloys have been dedicated to low alloys' dissimilar welding steels for high-strength applications [40]. Silva et al. [41] evaluated the microstructural features and mechanical properties of a novel Ni-

✉ Cleiton Carvalho Silva
cleiton@metalmat.ufc.br

[1] Department of Metallurgical and Materials de Engineering, Welding Research and Technology Laboratory, Universidade Federal do Ceará, Campus of Pici, Building 1080, Fortaleza, Ceará 60440-552, Brazil

based alloy developed for dissimilar joining applications. This alloy demonstrated some susceptibility to solidification cracking, depending on its dilution with the steels. Miná et al. [42] proposed a new approach to weld the API 5L X65 steel pipes with an internal cladding of alloy 625, using two different filler metals in the same joint to provide an overmatch of yield strength. The authors reported the nucleation of numerous solidification cracks and the first two steel weld passes, which significantly impaired the mechanical properties of the welded joint. In another study, Miná et al. [42] developed a new proposal for dissimilar girth welding of API 5L X65 steel pipe with an internal alloy 625. In this procedure, alloy 625 was replaced by alloy 22 to deposit the first two weld passes. This replacement assured the welded joint a high yield strength, and no solidification cracking was apparent. Solidification cracking is an ongoing problem, as demonstrated in the literature, and is an issue that has attracted the attention of various researchers.

Solidification cracks occur in the molten zone during the terminal stage of solidification (between 80 and 99% of the solid fraction) when the tensile stresses developed across the adjacent grains exceed the strength of the weld metal, almost completely solidified [43, 44]. This stress is an inherent factor in the metal solidification process and is related to the material's thermal contraction with the temperature drop. The presence of an extensive liquid phase film at the end of solidification is a characteristic of each material, and the higher the solidification temperature interval is, the more significant the portion of the liquid phase at the end of the solidification is, and, consequently, the higher the tendency to form such cracks [43, 44]. If the amount of liquid remaining is large enough near the crack region, it can fill the gaps created, thus "healing" them. This process is called backfilling and can be total or partial. In total backfilling, the liquid penetrates the entire crack and "heals" it completely, while in partial backfilling, only a part of the crack is healed [45].

The American Welding Society (AWS) defines weldability as the capacity of a material to be welded under fabrication conditions imposed into a specific, suitably designed structure and to perform satisfactorily in the intended service [ref]. In other words, this concept can be summarized as the susceptibility of materials to form solidification cracks. Various weldability tests can be used to evaluate the weld solidification cracking susceptibility. The Sigmajig Test assesses the solidification and liquation crack susceptibility [46]. The Hot Ductility Test simulates the HAZ of a given welding condition by imposing a thermal cycle on the material [47]. The Varestraint Test (or its variation, the Transverse-Varestraint Test, also known as Trans-Varestraint Test), where an augmented tensile strain is applied to the test specimen bending it to a controlled radius at an appropriate moment during the welding process [48, 49]. The most commonly used weldability tests nowadays are the Varestraint and the Trans-

Varestraint tests. Professor Carl D. Lundin developed the Varestraint test under Professor Warren F. Savage's guidance in 1965 [50, 51]. The Trans-Varestraint test was developed in Japan by researchers at Osaka University [52–54].

The nickel-based alloys are a class of materials with excellent corrosion resistance and good mechanical properties, but their usage is limited from an economic point of view due to their high cost. Moreover, due to their austenitic nature and solidification as a face-centered cubic (FCC) gamma phase, Ni-base alloys are inherently susceptible to weld solidification cracking [3]. Furthermore, dissimilar welding can make this characteristic even more likely; hence, the mixing of two different metals adds to the weld pool alloying elements that can induce the formation of brittle TCP phases that increase the solidification range increase the susceptibility to solidification cracks [4].

Inconel 625 and Hastelloy C-276 are examples of nickel-based alloys. The Inconel 625 is an Nb-bearing Ni-based alloy from the Ni-Cr-Mo family, which has been used extensively in applications requiring high-temperature strength and oxidation resistance. The solidification of the alloy 625 is highly influenced by the Nb, Si, and C in their chemical composition since these elements exhibit a strong tendency to form secondary phases at the end of the solidification process. The Hastelloy C-276 is a highly corrosion-resistant nickel-based alloy derived from the Ni-Cr-Mo ternary system, with W and Fe as additional alloying components. Molybdenum and Tungsten impart resistance to both oxidizing and reducing chemicals. Besides, their large atomic size, compared to that of nickel, provide a robust solid-solution strengthening effect [44].

The dissimilar welding between these nickel-based alloys and other materials such as carbon steels can contribute to the formation of detrimental TCP phases during the Fusion Zone solidification. For instance, considering the welding performed with the alloy 625, Fe and C content in the weld pool has different effects. The Fe increases the capability of forming the TCP Laves phase, which is detrimental to the material. The C helps the NbC carbides formation, decreasing the solidification temperature range and, consequently, the susceptibility to solidification crack formation [5]. Welding with the alloy C-276 in the presence of Cr, Mo, and Fe induces the formation of TCP σ phase while a higher content of W stabilizes the P and μ-phases, which are also detrimental [44].

The weldability of these alloys has been long studied, and in recent research, LIPPOLD et al. [55] compared the weldability of several nickel-based alloys, including 625. According to the authors, the 625 weld metal was the most susceptible to solidification cracking among all the other alloys tested, even though the manufacturing practice has shown that this filler metal is usually quite resistant to cracking—the crack "healing" mechanism explains this contradiction. CIESLAK et al. [56] compared the weldability of

three different Ni-Cr-Mo alloys, including Hastelloy C-276. Using the Varestraint test, the authors reported that the alloy with the least weldability was the C-276 due to the higher amount of secondary phases present at the end of the solidification process. ROWE et al. [57] compared the weldability of 625 and C-276 alloys using the Varestraint test. The authors reported that alloy C-276 has higher weldability than alloy 625.

However, even though nickel-based alloys' weldability is frequently studied, there is little research regarding the effect of the welding Ni-based alloys on carbon steels and the risk of solidification cracking. The absence of such investigations has motivated the development of a research project at the Welding Research and Technology Laboratory at the Universidade Federal do Ceará, Brazil. This study evaluates the influence of the base metal on the solidification cracking susceptibility of the Inconel 625 and Hastelloy C-276 alloys by applying the Trans-Varestraint test associating the behavior with the thermodynamic simulation according to the Scheil-Gulliver equation.

2 Experimental procedures

The Ni-based alloys used as filler metals in this investigation had by X-ray fluorescence spectroscopy their chemical composition obtained, using a handheld XRF spectrometer. The chemical compositions are shown in Table 1.

The base metals used in this investigation were the ASTM A36 and the AISI 1045 carbon steels, whose chemical compositions were obtained by optical emission spectroscopy and are shown in Table 2.

Samples for the Trans-Varestraint test were prepared by machining a groove at a specified position on a 100×210-mm plate of 12.5-mm width.

Before the machining process, the groove geometry was determined by measuring the height, the penetration, and the length of the transverse section of a bead made with the same welding conditions used for the Trans-Varestraint test, such as heat input, filler metals, and base metals. The exact geometry of the bead section was machined into the plates. A scheme of the samples is shown in Fig. 1.

The Trans-Varestraint test was used to determine the dissimilar welds' solidification crack susceptibility using the Ni-based filler metals and the carbon steel base metals.

This work presents an alternative method to perform the Trans-Varestraint test (TVT). The main difference is the deposition during the welding process. Usually, the TVT is executed using an autogenous process, such as gas tungsten arc welding (GTAW). Here, the filler metal was deposited into a groove, machined in the sample, during the test (Fig. 1). Thereby, the dissimilar weld's solidification crack susceptibility could be evaluated along with, for instance, the effect of dilution on the solidification crack behavior.

The volume of the material deposited must be as close as possible to the groove volume to guarantee that there should be the as little formation of reinforcement during the deposition as possible, as demonstrated in Fig. 2 that shows an actual specimen after the Trans-Varestraint test.

All the other TVT parameters were maintained unchanged, and the test dynamics remained the same. During the welding, the sample is forced in a downward bending motion, which is initiated by applying a load on the loading rollers, which forces the plate to conform to the die block radius. The die block radius determines the strain applied during the test. Thereby allowing a relationship between strain and cracking susceptibility to be determined [3]. In this investigation, the solidification cracking susceptibility was evaluated by measuring the maximum crack length (MCL), and the total crack length (TCL) on the surface of the sample tested at a given strain. All tests were performed in duplicate.

The welds were carried out by depositing the Ni-based alloy filler metals onto samples of two different carbon steel. A full factorial experimental design was carried out in this study, using the filler metal as the first control factor with two levels: Hastelloy C-276 and Inconel 625; the second was the base metal also with two levels: ASTM A36 steel and AISI 1045; the third was the heat input: 0.75 and 1.25 kJ/mm; and the fourth control factor was the strain with three levels: 0.5, 1.0, and 3.0%; thus making a total of 24 tests for each set. Four different sets of samples, considering the combination of filler and base metal, were evaluated and are shown in Table 3. Each test with a code was identified, as shown in Table 3. This code will be used throughout the document to identify the set of samples.

The welding parameters applied in this study are shown in Table 4. The shielding gas used in the tests was composed of 75% argon + 25% helium, with a flow rate of 20L/min. Table 5 presents the Trans-Varestraint test parameters.

After the tests, the samples were polished and photographed at ×40 magnification. The cracks were

Table 1 Chemical composition (wt%) of the Ni-based filler metals

Elements (wt%)	Ni	Cr	Mn	Fe	Mo	W	Nb	Ti	V	Co	Ta
IN625	65.2	21.5	-	0.40	8.8	-	3.72	0.15	0.06	0.07	0.02
C-276	59.2	16.02	0.37	5.36	15.3	3.35	-	0.09	0.02	0.12	-

Table 2 Chemical composition (wt%) of the carbon steel base metals

Elements (wt%)	C	Si	Mn	P	S	Ni	Cr	Mo	Cu	Nb	Al	V	Ti	Fe
AISI1045	0.49	0.18	0.64	0.015	0.014	0.015	0.012	0.005	0.001	0	0.037	0.003	0.003	base
ASTM A36	0.23	0.03	0.63	0.021	0.011	0.014	0.009	0.006	0.002	0.001	0.058	0.004	0.002	base

measured using the ImagePro Plus® software. After this step, the samples were cut transversally to the crack propagation direction to examine the crack penetration, as shown in Fig. 2B. The sectioned samples were then conventionally prepared for metallographic analysis. Energy dispersive of X-ray spectroscopy (EDS) analyses coupled to an FEI Quanta 250 scanning electron microscope was performed to evaluate the Fusion Zones' composition.

The Scheil-Gulliver solidification diagrams were calculated using the JMatPro® (10.2 version) software. The Scheil diagram allows the essential factors in the assessment of the susceptibility to the formation of solidification cracks, such as the BTR (Brittle Temperature Range) and the solidification temperature range of the Fusion Zone, to be estimated.

Analysis of variance (ANOVA) tests was performed with the software Statistica on the crack measurements from the Trans-Varestraint tests. The results defined the parameters that influenced the crack propagation during the Trans-Varestraint tests. The parameters evaluated by the ANOVA tests were applied strain, base metal, nickel base wire, and heat input.

3 Results and discussion

3.1 Result of ANOVA tests

Cracks formed during the Trans-Varestraint tests are shown in Fig. 3, with cracks on the surface. All samples were evaluated,

and the MCL and TCL were determined. Based on the crack lengths obtained by the Trans-Varestraint test, ANOVA tests were performed to define which control factors used in the set of experiments were able to influence the susceptibility to solidification cracking and what was de "degree" of this influence. Based on this information, it is possible to define which parameters cause greater or lesser variations in the weldability of the set, indicating which of them should be avoided or controlled in joints with similar compositions. The results obtained with the ANOVA test are shown in Table 6. P values lower than 0.05 indicate that the control factor evaluated influences the crack length.

The P values obtained by the ANOVA test show that the heat input does not influence the results of the Trans-Varestraint tests performed with the two wires. The highest energy used was 67% higher than the lowest heat input. However, with this range of heat input, the energy intensity combined with other factors may not have been sufficient to cause significant effects on weldability.

Table 7 shows the dilution values for each fusion zone. The dilution calculation was done by the relationship between each wires' chemical compositions and the fusion zone itself, based on EDS measurements made in samples tested with 1.0% strain. Table 7 shows that all the Fusion Zones have a dilution below 10%, i.e., less than 10% of the fusion zone was composed of base metal. The low dilution levels obtained, even with the highest heat input applied, explains why the heat input variation did not cause any effect on the

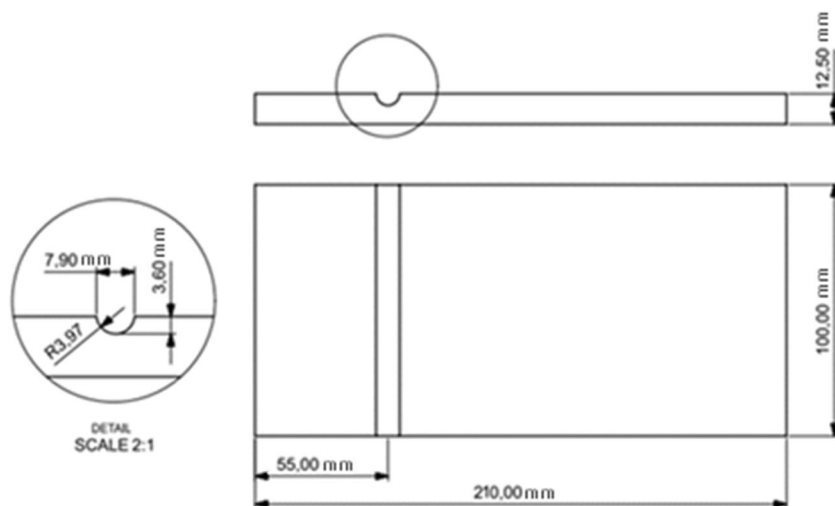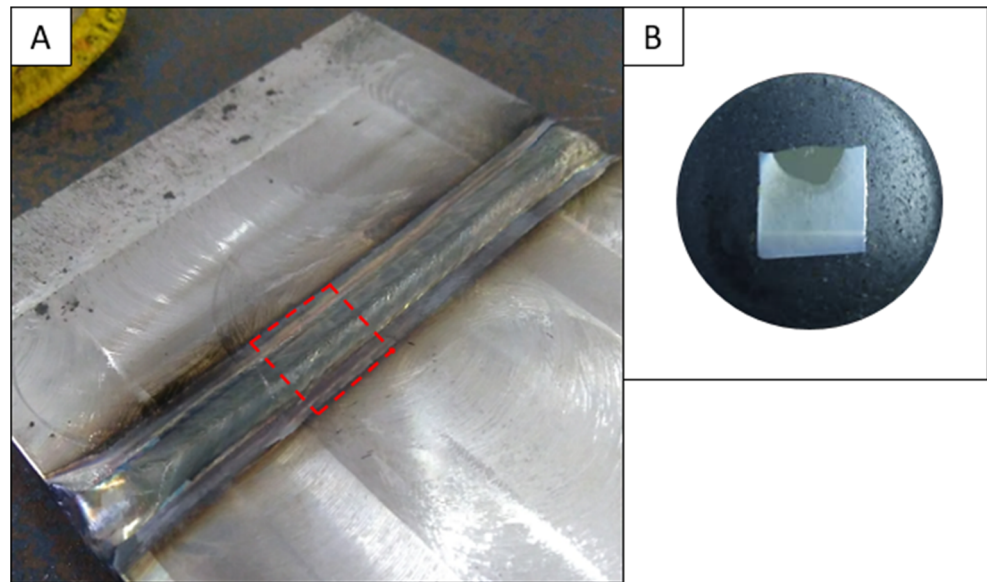**Fig. 1** Scheme of the sample used at the Trans-Varestraint test

Fig. 2 **A** Joint after the alternative Trans-Varestraint test: the red dotted lines indicate the specimen extraction place. **B** Example of specimen extracted from joint

weldability, considering the different sets of samples evaluated. The low dilution levels only cause slight variations in the Fusion Zone compositions, and those variations were not significant to cause any substantial changes in the solidification behavior of the material.

New alloying elements should be introduced to the weld pool during the welding process, such as Fe and C from the base metal, if a higher dilution level was achieved. These elements can be very detrimental to the weldability of the material since they can significantly change the resulting microstructures in the fusion zone, thus promoting the formation of terminal secondary constituents that increase the solidification temperature range of the material [44, 58, 59]. For instance, the addition of iron and carbon in 625 alloys furthers the formation of low-temperature precipitates, such as the Laves phase and carbides, respectively [16, 60, 61]. For Ni-Cr-Mo alloys, like C-276, iron addition facilitates the formation of the σ phase, a TCP detrimental phase that also precipitates at low temperatures [44]. Besides, it is well known that the cracking tendency of weld metals increases with the widening in the solidification temperature range and the formation of terminal secondary constituents in small quantities [55, 56, 60].

Table 3 Combination of alloys used in the Trans-Varestraint test

Wire	Base metal	Pair code
Hastelloy C-276	ASTM A36	C-276/A36
	AISI 1045	C-276/1045
Inconel 625	ASTM A36	625/A36
	AISI 1045	625/1045

The solidification process of the dissimilar welding between nickel-base alloys and carbon steel for high dilution levels can be estimated by simulation and has also been investigated.

The low dilution level may be one of the reasons to explain why the variation in heat input did not influence the weldability of the dissimilar welds. The heat input variation for dissimilar welds tested changed the dilution within a range that did not impair the fusion zone's solidification (2.8 to 8.7%), as shown in Table 7.

Low variation in dilution can be attributed to the fact that the heat input level has been changed by modifying travel speed, which does not affect the penetration of the weld bead compared to modifications in weld current. In fact, in this procedure, the heat input is governed by the amount of heat transferred per length unit due to the travel time associated with the welding speed. In this case, there is an association with the deposition rate intrinsic of the GWAW process. The lower the welding speed, the more filler metal is deposited per unit length, increasing the weld pool's volume and creating a barrier effect between the arc and the substrate [11]. This barrier effect has difficulty the melting of the bottom of the groove, reducing the dilution level. Thus, no significant change in the dilution of the fusion zone was found.

On the other hand, if the welding is current-controlled the heat input variation, they should have more relevant results regarding the variation in dilution, as the increase in heat input given by the arc power promotes a series of essential effects. One effect is an increase in the electric arc temperature, which causes an increase in the temperature of the liquid metal in the molten pool [11]. These aspects affect the convective movement of the fusion pool, which results in greater penetration than that obtained by decreasing the welding speed, which

Table 4 Welding parameters

Heat input	Travel speed	Current	Time	Alimentation speed
0.75 kJ/mm 1.25 kJ/mm	42 cm/min 25.25 cm/min	I_p= 300A / I_b = 120A	t_p = 2.2ms / t_b = 4ms	10m/min

would increase the dilution of the fusion zone. Further investigations will be carried out to evaluate this aspect.

The crack formation results were evaluated based on the MCL, or maximum crack length, which is the length of the most significant crack formed during the Trans-Varestraint test [62]. This maximum distance propagated by a solidification crack is dependent on the Mushy Zone length. This zone is defined as the region where solid dendrites (columnar or equiaxed) and liquid phases coexist and is the brittle area that enables the formation of cracks during the application of stress [43]. Therefore, the Mushy Zone extension can be correlated to the quantity of remaining liquid at the end of the solidification process. It can be stated: as the greater the amount of liquid remaining at the end of the solidification, the longer the Mushy Zone will be, and, consequently, the Trans-Varestraint test will indicate higher MCL values leading to a result of lower weldability.

For instance, Cieslak et al. compared the weldability of three Ni-Cr-Mo alloys, C-4, C-22, and C-276 — the latter is also a topic of the present study. According to the authors, the C-276 alloy showed the least weldability among the alloys tested due to the more significant amount of secondary phases formed at the end of the solidification, which resulted in higher MCL values [56]. However, it is essential to say that if the liquid phase content is high enough for the backfilling process to occur, then the cracking susceptibility would start to decrease [60]. Lippold et al. already identified this phenomenon when investigating the weldability of pure 625 alloys. In that study, the authors reported that for weld metals that achieve resistance to solidification cracking through a crack backfilling mechanism, the Varestraint test might not accurately reflect their susceptibility to cracking [55].

The dilution between the nickel-based alloys and other materials such as steel can also influence crack propagation and weldability, depending on the dilution level. For instance, a study carried out by Dupont et al. investigated the dilution of

the nickel-based alloys Inconel 622 and Inconel 625, diluted with AL-6XN super austenitic stainless steel. The authors reported that welds prepared with IN625 had the lowest resistance to hot cracking, and the cracking susceptibility increased with decreasing dilution. In contrast, welds prepared with IN622 were more resistant to solidification cracking, and the cracking susceptibility, in this case, was not particularly sensitive to the dilution level [59].

Based on the crack measurements carried out on the weld surface of the Trans-Varestraint samples, an ANOVA statistic test was performed, and the result has shown that changing the base metals has influenced the crack length only for the C-276 alloy. Figures 4 and 5 show the MCL's behavior for tests carried out with heat input equal to 0.75 kJ/mm and 1.25 kJ/mm, respectively. There is no significant variation in crack length with heat input change. For the alloy C-276, the tests carried out with AISI 1045 steel showed a larger crack size than those carried out with ASTM A36 steel for all strain levels applied. This behavior indicates that among the base metals used, the AISI 1045 steel is the one that causes the largest crack size in the alloy C-276, resulting in the least weldability. This result suggests that a more significant amount of secondary phase precipitation occurred during the Fusion Zone solidification, allows the formation of longer cracks during the Trans-Varestraint test, when the weld metal is composed of the alloy C-276 and 1045 steel. For the Inconel 625, the use of AISI 1045 or ASTM A36 carbon steel did not cause any significant variation on the crack size obtained with the Trans-Varestraint test, indicating that both base metals promoted equivalent weldabilities.

The strain used for the Trans-Varestraint tests influenced the crack length for both nickel-based alloys. That was an expected result since the strain is one of the most critical variables present in the Trans-Varestraint test.

Table 8 shows the ANOVA results for both base metals used. The results show that, for the ASTM A36 steel, the alloy used was irrelevant, and the crack sizes formed during the Trans-Varestraint test were equivalent for the alloy 625 and alloy C-276 wires. However, for the AISI 1045 steel, the crack size is influenced by the Ni-based alloy used since, for MCL analysis, the P-value was below 0.05.

Figure 6 compares MCL results obtained by Cieslak et al. (1986) for the C-276 nickel-based alloy and the MCL results obtained by the Trans-Varestraint tests for the C-276 nickel-based alloy diluted in ASTM A36 and AISI 1045. The

Table 5 Trans-Varestraint test parameters

Strain	Weld length	Bend position	Bend orientation
0.5% 1% 3%	10mm	60mm from start	Transverse

Fig. 3 Examples of cracks formed during the Trans-Varestraint test with heat input equal to 1.25kJ/mm in the fusion zones composed by C-276/A36 (**A**); C-276/1045 (**B**); IN625/A36 (**C**); and IN625/1045 (**D**)
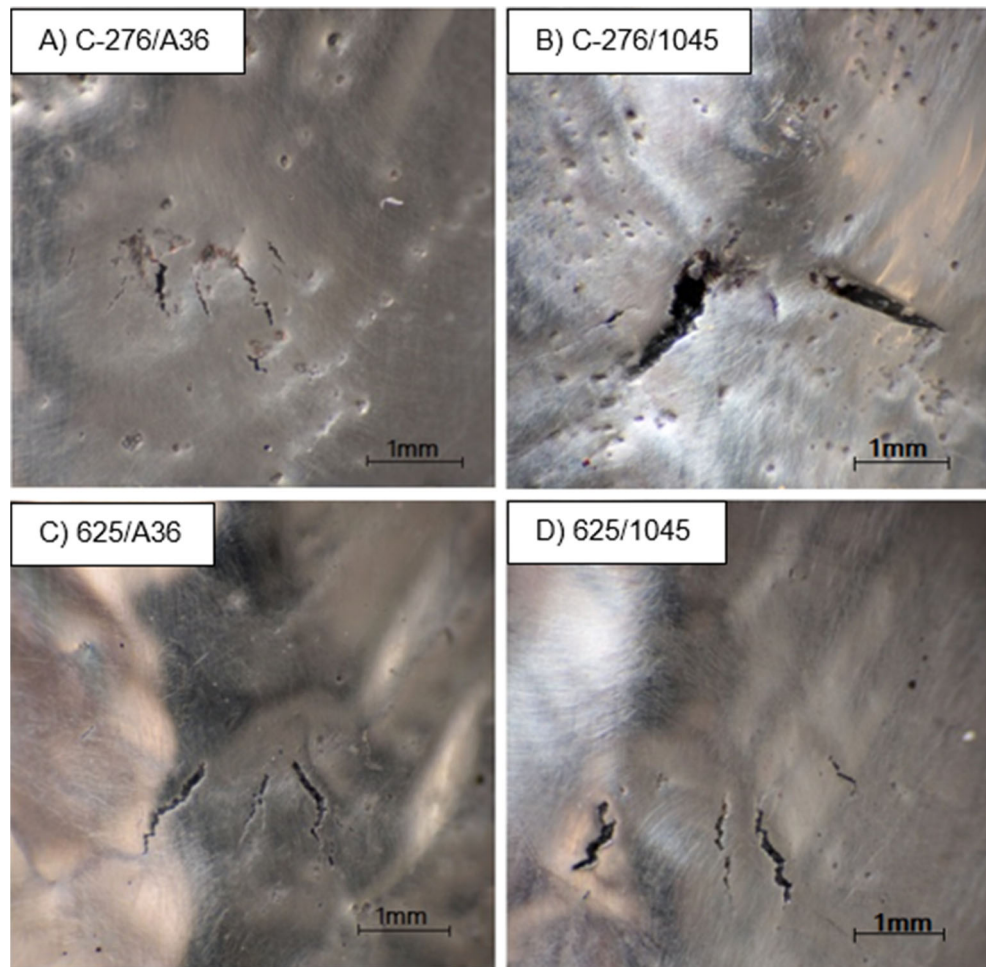
comparison shows there is an increase in MCL when this alloy is diluted with carbon steel. Additionally, the higher the percentage of carbon in the base metal is, the higher the MCL is.

Figure 7 shows the same approach taken previously with the C-276 alloy and compares the MCL results obtained by Lippold et al. (2008) for pure 625 nickel-based alloy and the MCL results of the Trans-Varestraint tests carried out in this study for the alloy 625 diluted with ASTM A36 and AISI

1045 steels. The alloy 625 presents a different behavior than the C-276 alloy, showing no difference in MCL results from pure 625 alloy and dissimilar welds, considering the dilution range achieved in this study.

3.2 Dilution simulation

Aiming to verify the solidification path of the same set of experiments studied considering higher dilution levels and

Table 6 ANOVA results for Hastelloy C-276 and Inconel 625 wires. P values lower than 0.05 are in italics

Treatment	Crack length	P	
		C-276	IN625
Heat input	MCL	0.419752	0.244928
	TCL	0.282492	0.073552
Base metal	MCL	*0.000217*	0.556908
	TCL	*0.049749*	0.984433
Strain	MCL	*0.013771*	*0.000041*
	TCL	*0.000022*	*0.000007*

Table 7 Dilution of Fuzion Zones welded with different heat inputs

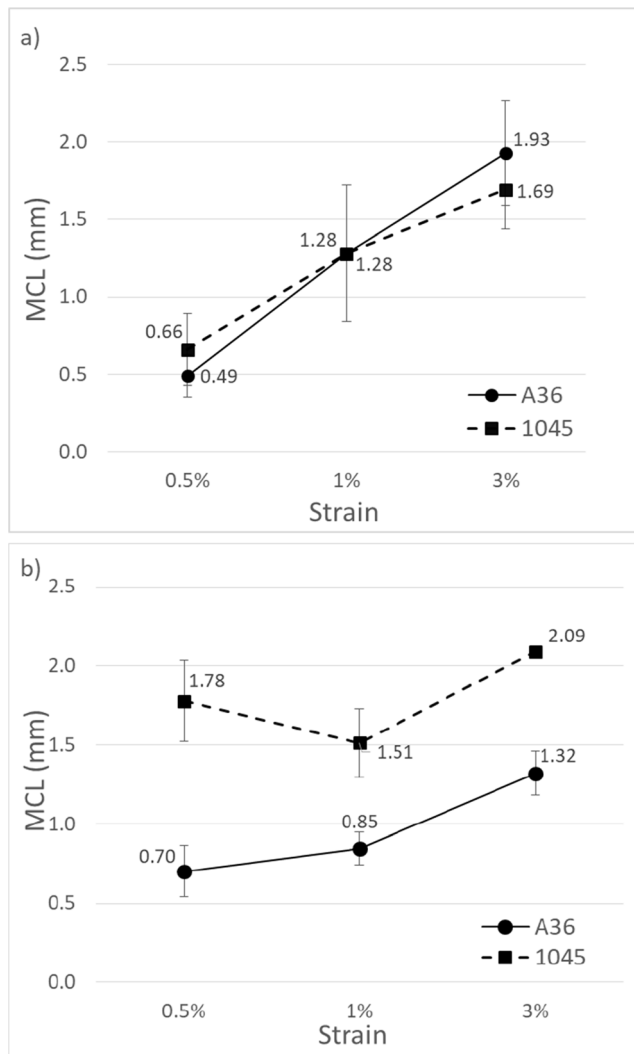| Sample	Dilution
625/A36-0.75kJ/mm	7.5%
625/A36-1.25kJ/mm	3.8%
625/1045-0.75kJ/mm	8.7%
625/1045-1.25kJ/mm	4.7%
C-276/A36-0.75kJ/mm	8.7%
C-276/A36-1.25kJ/mm	4.98%
C-276/1045-0.75kJ/mm	6.9%
C-276/1045-1.25kJ/mm	2.8%

Fig. 4 MCL results of Trans-Varestraint tests performed with a heat input of 0.75kJ/mm and Inconel 625 wire (**a**) and Hastelloy C-276 wire (**b**)
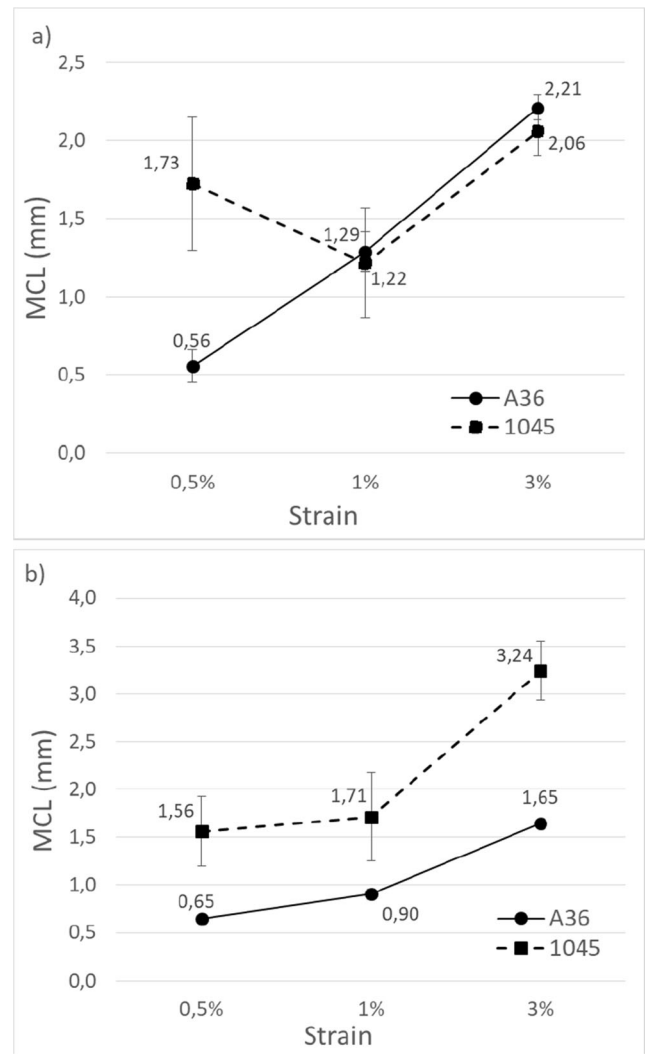

Fig. 5 MCL results of Trans-Varestraint tests performed with a heat input of 1.25kJ/mm and Inconel 625 wire (**a**) and Hastelloy C-276 wire (**b**)

their influence on the solidification cracking susceptibility based on parameters like solidification temperature range and BTR, new compositions were calculated for each combination between alloy and steel, supposing dilutions ranging from 5 to 40%.

Scheil diagrams simulated for the alloys 625 and C-276 used in the present work are shown in Fig. 8. The phases formed at the end of the solidification process, and their volume fractions and precipitation temperatures were estimated based on the data and the plotted diagram. Additionally, the information on starting and ending solidification temperatures and the variation for each solid phase fraction formed during the solidification were also predicted.

The results for each filler/base metal set are shown in Fig. 9. Both alloys showed an increase in the secondary phase fraction with increasing dilution, which was expected since, with the more significant presence of the base metal in the Fusion Zone, new alloy elements, such as C and Fe, should

be incorporated into the weld pool, promoting the formation of new phases.

The graphs (a), (b), (c), and (d) in Fig. 9 present the data obtained with Hastelloy C-276 alloy diluted in the ASTM A36 and AISI 1045 steel plates. The predicted secondary phases that would precipitate during the solidification process are σ and M_6C carbides for all dilution levels tested, and P phase for dilution levels equal or less than 5%. Evaluating both graphs' behavior shows that the presence of AISI 1045

Table 8 ANOVA results for AISI 1045 and ASTM A36 base metals. P values lower than 0.05 are in italics

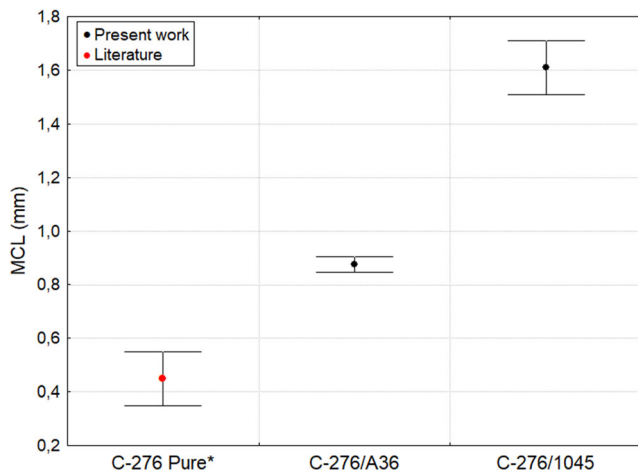| Base metal	Crack length	P
AISI 1045	MCL	*0.036459*
	TCL	0.189635
ASTM A36	MCL	0.225237
	TCL	0.552259

Fig. 6 Comparison between MCL results obtained by Cieslak et al. (1986) for the C-276 nickel-based alloy and the MCL results obtained by the Trans-Varestraint tests for the C-276 nickel-based alloy diluted in ASTM A36 and AISI 1045. *Data regarding pure Hastelloy C-276 alloy extracted from Cieslak et al. (1986)

steel in combination with C-276 alloy causes a more significant increase of the secondary phase fraction compared to the C-276/A36 set. For instance, when ASTM A36 steel is the base metal, the total fraction of the secondary phase at the end of solidification with a 40% dilution is approximately 12.5%, while for the AISI 1045 base metal, this value is 22%. This result shows a more significant induction of secondary phase precipitation in the welded joints of alloy C-276 with the carbon steel AISI 1045 than with the ASTM A36 steel. Once again, we can cite the work developed by Dupont et al. [59], where the authors investigated the dissimilar welding between the alloys IN622 — similar to C-276 alloy — and the super austenitic stainless steel AL-6XN (24.2%Ni, 21.6%Cr,
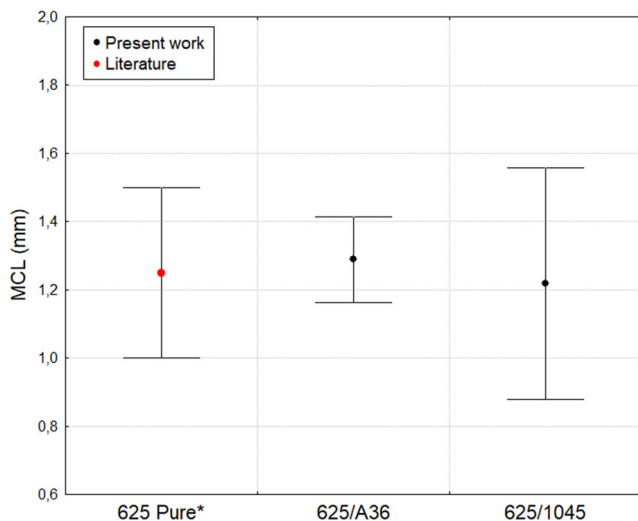
Fig. 7 Comparison between MCL results obtained by Lippold et al. (2008) for the 625 nickel-based alloy and the MCL results obtained by the Trans-Varestraint tests for the 625 nickel-based alloy diluted in ASTM A36 and AISI 1045. *Data regarding pure Inconel 625 alloy extracted from Lippold et al. (2008)
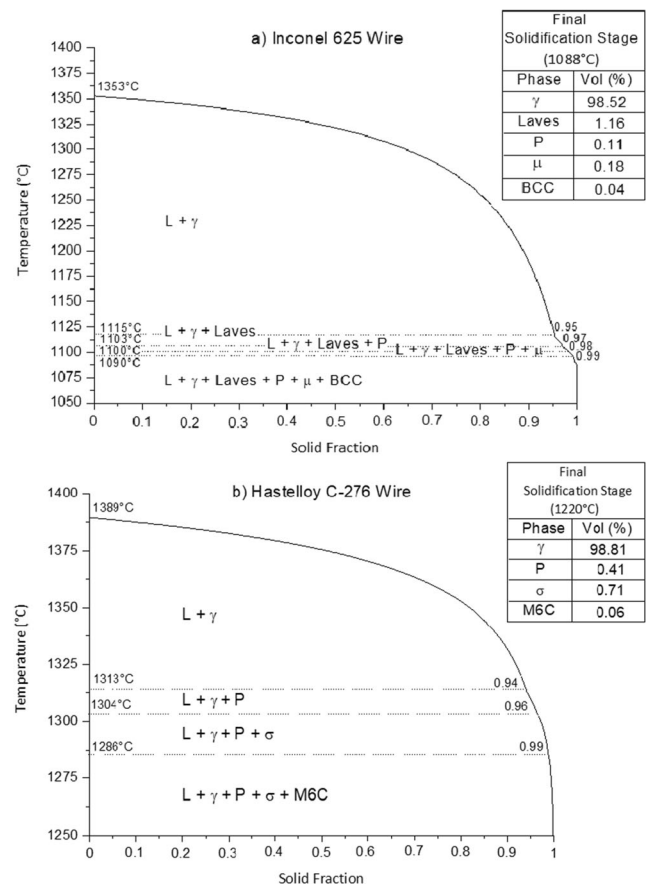

Fig. 8 Examples of the Scheil diagram simulated for Inconel 625 alloy (**a**) and C-276 alloy (**b**) wires

6.1%Mo, and 0.02%C), which has a higher alloying element content than the carbon steels. However, in this case, the higher C content can be ignored for comparisons. The authors state that the AL-6XN/IN622 welds exhibit a two-step solidification process, consisting of L → γ followed by L → (γ + σ). According to the authors, the L → (γ + σ) reaction temperature in AL-6XN/IN622 welds depends on the dilution level and ranges from 1354°C for "pure" AL-6XN to 1285°C for "pure" IN622. Comparing the results obtained by Dupont et al. [59] and the ones obtained in the present work, some similarities can be identified. As the base metal used by Dupont et al. [59] has less carbon, it does not promote the precipitation of carbides as was predicted for the dissimilar welding between C-276 alloy and carbon steels, and as proposed in the present work.

Simulations of the solidification process also allow the prediction of essential characteristics, such as the BTR and the solidification range (ΔTsol). The BTR was estimated by subtracting the temperature values found when the solid fraction is equal to 80% and 99% during the solidification process, as pointed out by Santillana et al. [57]. At this interval, because a segregated liquid film still exists between the dendrites, a minor strain leads to cracking [57]. The wider the
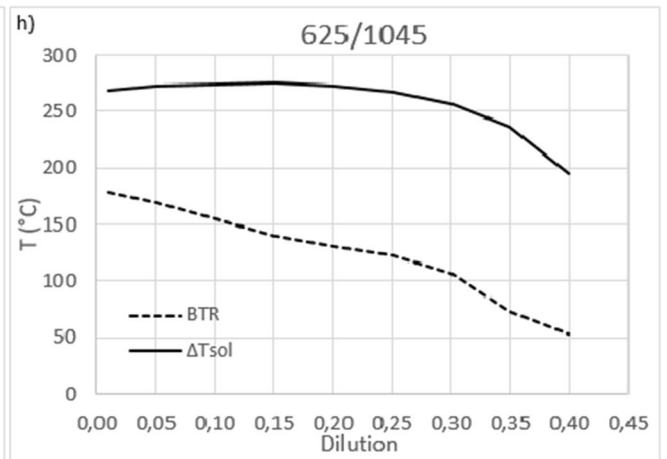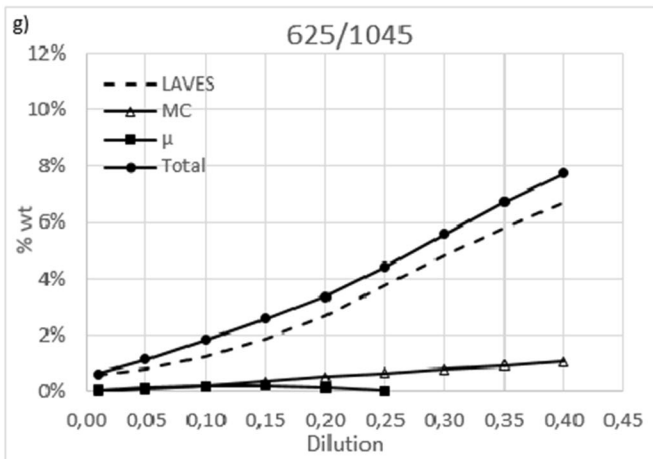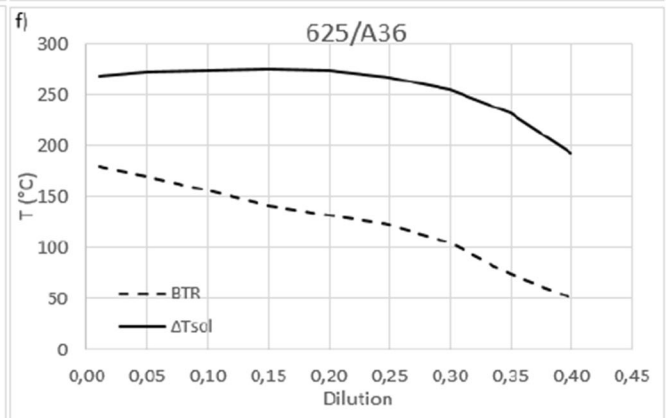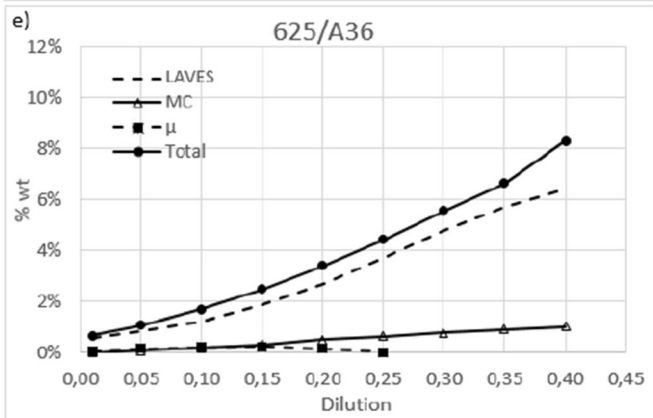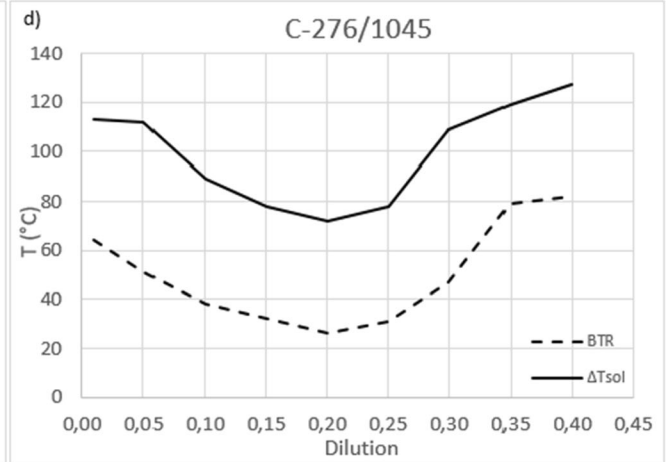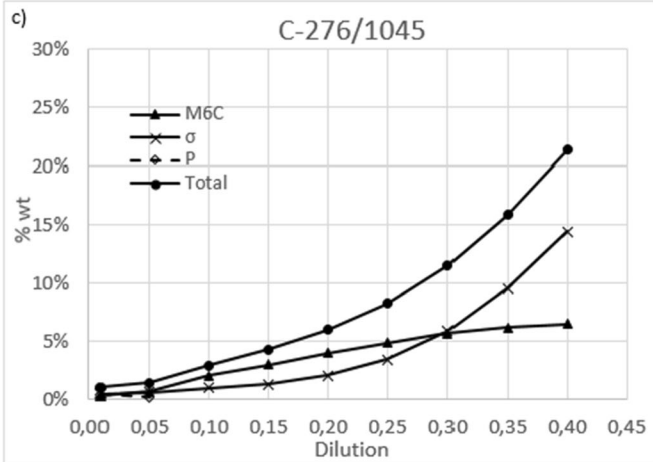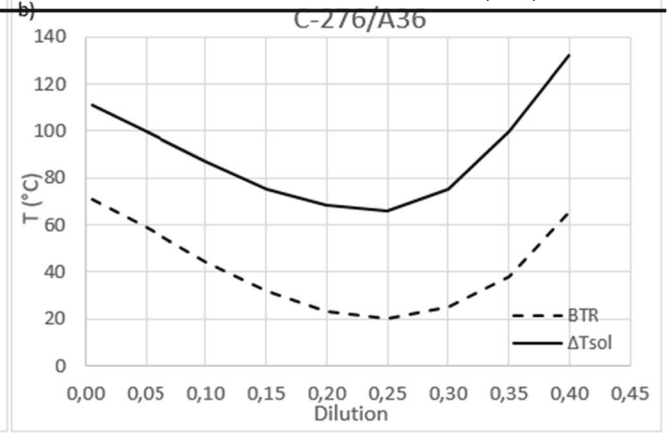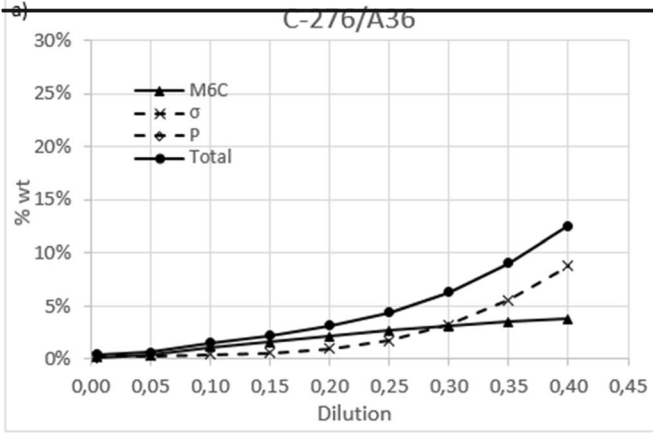
◀ **Fig. 9** Simulation results obtained by varying the dilution from 0 to 45% and with a heat input of 0.75kJ/mm for the sets %wt versus dilution for C-276/A36 (**a**); temperature versus dilution for C-276/A36 (**b**); %wt versus dilution for C-276/1045 (**c**); temperature versus dilution for C-276/1045 (**d**); %wt versus dilution for 625/A36 (**e**); temperature versus dilution for 625/A36 (**f**); %wt versus dilution for 625/1045 (**g**); and temperature versus dilution for 625/1045 (**h**)

range, the longer (at a constant cooling rate) the semisolid material stays in this critical range and the greater the stress concentration is, resulting from the thermal contraction restriction [57]. The greater the BTR, the greater the susceptibility to solidification cracking is [43, 57].

According to the results, variations in the dilution level promoted changes in the features evaluated, as shown in Fig. 9. The curves indicate that the BTR and ΔTsol values have very similar behavior, presenting a "U" shape, with an inflection point at 25% of dilution for the A36 steel base metal and 20% dilution 1045 steel base metal. Comparing this behavior with the secondary phases behavior presented in the chart shows that after reaching the inflection point dilution, the σ-phase amount increases significantly. At the same time, there are no significant changes in the amount of precipitated M_6C carbide. The σ phase usually forms at lower temperatures than the M6C carbide, and its formation in larger amounts will probably cause an enlargement of the ΔTsol range and, consequently, an increase of the BTR as well. Evaluating both graphs shows that when the percentage of σ phase exceeds the amount of M6C carbides, there is a rapid increase in BTR and ΔTsol, which means that the susceptibility of the material to form solidification cracks increases.

Graphs (e), (f), (g), and (h) in Fig. 9 present the data obtained from Inconel 625 alloy diluted in the ASTM A36 and AISI 1045 steel plates. The simulations performed with the Inconel 625 alloy did not vary significantly between the two base metals. However, it shows an increase in the fraction of the secondary phase with increasing dilution. This information means that, when increasing the dilution, there should probably be a decrease in weldability, since the increasing amounts of solute-enriched liquid (which becomes secondary phases) lead to an increase in the susceptibility to solidification cracking as it impairs the formation of solid/solid boundaries, thus avoiding the accommodation of a shrinkage strain across the boundaries [44]. The predicted secondary phases that should precipitate during the solidification process were Laves and carbides MC for all dilution levels and μ-phase for dilution levels equal or less than 25%. In the study developed by Dupont et al. [59] already quoted in the present work previously, the authors reported that welds prepared with IN625 and the super austenitic stainless steel AL-6XN exhibit a three-step solidification process consisting of L → γ, L → (γ + NbC), and L → (γ + Laves) [59]. Several other authors also identified the precipitation of the same secondary phases

when studying the solidification of the alloy 625 [16, 44, 59, 61, 63]. However, the μ-phase precipitation during the solidification of t36he alloy 625 has not been reported in the literature until now.

The values of BTR and ΔTsol decreased with the increase of the secondary phase fraction. This behavior occurs because, with the increase in dilution, there is also greater availability of alloying elements in the fusion zone. During the solidification process, the remaining liquid becomes enriched more quickly, allowing the secondary phase's occurrence at higher temperatures. As a consequence, there is a decrease in BTR and ΔTsol values.

4 Conclusions

Based on the experimental and computational results obtained in the present study about the weldability of dissimilar assemblies between nickel-based alloys — Hastelloy C-276 and Inconel 625 — and carbon steels — ASTM A36 and AISI 1045 — using the Trans-Varestraint test with the variation of heat input and deformation, we can conclude that:

a. The Ni-based alloy that presented the most variability in weldability depending on the base metal used was the Hastelloy C-276. Among the tested joints, the one with the least weldability was composed by Hastelloy C-276 + AISI 1045, which can be explained by the greater amount of secondary phase formed during the solidification process predicted by the simulation test for this materials combination, inducing the formation of solidification cracks.

b. The weldability results obtained for the Inconel 625 + ASTM A36 set and Inconel 625 + AISI 1045 set were very similar, indicating that the weldability of this nickel-based alloy was not influenced by the base metal changing, fact that was confirmed by the ANOVA tests. This result can be related to the low dilution obtained during the Trans-Varestraint test. However, the simulation tests showed that even increasing the dilution level, the amount of secondary phases of both pairs would remain similar, indicating that the weldability should not variate much between sets with those material combinations even with an increased dilution level.

c. The heat input levels tested were too alike to cause any variation at the joint dilution and, consequently, at the Fusion Zone composition. Because of the similarity between the Fusion Zones' compositions, there was no significant variation of weldability with heat input. Probably, if the heat input had interfered more intensely on the dilution levels, there should be considerable differences in the joint's behavior during the solidification process. The

ANOVA tests confirmed the non-interference of the heat input levels variation on the weldability of different sets.

References

1. Maltin CA, Galloway AM, Mweemba M (2014) Microstructural evolution of Inconel 625 and Inconel 686CPT weld metal for clad carbon steel linepipe joints: a comparator study. Metall Mater Trans A 45(8):3519–3532. https://doi.org/10.1007/s11661-014-2308-z

2. Kim JS, Lee HW (2016) Effect of welding heat input on microstructure and texture of Inconel 625 weld overlay studied using the electron backscatter diffraction method. Metall Mater Trans A 47(12):6109–6120. https://doi.org/10.1007/s11661-016-3754-6

3. Hosseini HS, Shamanian M, Kermanpur A (2011) Characterization of microstructures and mechanical properties of Inconel 617/310 stainless steel dissimilar welds. Mater Charact 62(4):425–431. https://doi.org/10.1016/j.matchar.2011.02.003

4. Kourdani A, Derakhshandeh-Haghighi R (2018) Evaluating the properties of dissimilar metal welding between Inconel 625 and 316L stainless steel by applying different welding methods and consumables. Metall Mater Trans A 49(4):1231–1243. https://doi.org/10.1007/s11661-018-4469-7

5. Ranjbar K, Dehmolaei R, Amra M, Keivanrad I (2018) Microstructure and properties of a dissimilar weld between alloy 617 and A387 steel using different filler metals. Welding in the World 62(6):1121–1136. https://doi.org/10.1007/s40194-018-0610-x

6. Silva CC, Afonso CR, Ramirez AJ, Motta MF, Miranda HC, Farias JP (2016) Assessment of microstructure of alloy Inconel 686 dissimilar weld claddings. J Alloys Compd 684:628–642. https://doi.org/10.1016/j.jallcom.2016.05.231

7. Miná ÉM, Silva YCD, Dille J, Silva CC (2016) Effect of dilution on the microstructure of AWS ER NiCrMo-14 weld overlay deposited by TIG cold wire feed process. Soldagem & Inspeção 21(3):317–329. https://doi.org/10.1590/0104-9224/SI2103.07

8. Silva CC, Afonso CRM, Ramirez AJ, Motta MF, Miranda HCD, Farias JP (2012) Metallurgical aspects of dissimilar weld overlays of inconel 625 nickel based superalloys. Soldagem & Inspeção 17(3):251–263. https://doi.org/10.1590/S0104-92242012000300009

9. Rozmus-Górnikowska MAGDALENA, Cieniek Ł, Blicharski M, Kusiński J (2014) Microstructure and microsegregation of an Inconel 625 weld overlay produced on steel pipes by the cold metal transfer technique. Arch Metall Mater 59. https://doi.org/10.2478/amm-2014-0185

10. Silva CC, De Albuquerque VHC, Miná EM, Moura EP, Tavares JMR (2018) Mechanical properties and microstructural characterization of aged nickel-based alloy 625 weld metal. Metall Mater Trans A 49(5):1653–1673. https://doi.org/10.1007/s11661-018-4526-2

11. CC S (2013) Weld overlay. In: Wang, Q. Jane, Chung, Yip-Wah. (Org.). Encyclopedia of tribology 1edNew York: Springer US 1: 4094–4101

12. Jeshvaghani RA, Harati E, Shamanian M (2011) Effects of surface alloying on microstructure and wear behavior of ductile iron surface-modified with a nickel-based alloy using shielded metal arc welding. Mater Des 32(3):1531–1536. https://doi.org/10.1016/j.matdes.2010.10.006

13. Amudha A, Shashikala HD, Nagaraja HS (2019) Corrosion protection of low-cost carbon steel with SS-309Mo and Inconel-625 bimetallic weld overlay. Materials Research Express 6(4):046523. https://doi.org/10.1088/2053-1591/aafba6

14. Miná ÉM, Da Silva YC, Dille J, Silva CC (2016) The effect of dilution on microsegregation in AWS ER NiCrMo-14 alloy welding claddings. Metall Mater Trans A 47(12):6138–6147. https://doi.org/10.1007/s11661-016-3786-y

15. Longlong G, Hualin Z, Shaohu L, Yueqin L, Xiaodong X, Chunyu F (2016) Formation quality optimization and corrosion performance of Inconel 625 weld overlay using hot wire pulsed TIG. Rare Metal Mater Eng 45(9):2219–2226. https://doi.org/10.1016/S1875-5372(17)30006-1

16. Silva CC, De Miranda HC, Motta MF, Farias JP, Afonso CRM, Ramirez AJ (2013) New insight on the solidification path of an alloy 625 weld overlay. Journal of Materials research and Technology 2(3):228–237. https://doi.org/10.1016/j.jmrt.2013.02.008

17. Alexandrov BT, Lippold JC, Sowards JW, Hope AT, Saltzmann DR (2013) Fusion boundary microstructure evolution associated with embrittlement of Ni–base alloy overlays applied to carbon steel. Welding in the World 57(1):39–53. https://doi.org/10.1007/s40194-012-0007-1

18. Frei J, Alexandrov BT, Rethmeier M (2018) Low heat input gas metal arc welding for dissimilar metal weld overlays part II: the transition zone. Welding in the World 62(2):317–324. https://doi.org/10.1007/s40194-017-0539-5

19. Rajkumar V, Arjunan TV, Kannan AR (2019) Metallurgical and mechanical investigations of Inconel 625 overlay welds produced by GMAW-hardfacing process on AISI 347 pipes. Materials Research Express 6(7):076534. https://doi.org/10.1088/2053-1591/ab11f0

20. Solecka M, Kopia A, Radziszewska A, Rutkowski B (2018) Microstructure, microsegregation and nanohardness of CMT clad layers of Ni-base alloy on 16Mo3 steel. J Alloys Compd 751:86–95. https://doi.org/10.1016/j.jallcom.2018.04.102

21. Rajkumar V, Arjunan TV, Kannan AR (2020) Investigations on hardfacing and wear characteristics of nickel-based Inconel 625 overlaid welds over AISI 347 pipe. J Braz Soc Mech Sci Eng 42(1):12. https://doi.org/10.1007/s40430-019-2092-1

22. Farias FWC, da Cruz Payão Filho J, da Silva Júnior DA, de Moura RN, Rios MCG (2019) Microstructural characterization of Ni-based superalloy 625 clad welded on a 9% Ni steel pipe by plasma powder transferred arc. Surf Coat Technol 374:1024–1037. https://doi.org/10.1016/j.surfcoat.2019.06.084

23. Antoszczyszyn TJ, Paes RMG, Oliveira ASCMD, Scheid A (2014) Impact of dilution on the microstructure and properties of Ni-based 625 alloy coatings. Soldagem & Inspeção 19(2):134–144. https://doi.org/10.1590/0104-9224/SI1902.05

24. Diaz VV, Dutra JC, D'Oliveira ASCM (2012) Hardfacing by plasma transfer arc process. Weld Int 26(2):87–95. https://doi.org/10.1590/S0104-92242010000100006

25. Chattopadhyay P, van der Mee V, Zhang Z (2019) Hybrid electroslag cladding (H-ESC): an innovation in high speed electroslag strip cladding. Welding in the World 63(3):663–672. https://doi.org/10.1007/s40194-018-00692-y

26. Sandes SS, Alvarães CP, Mendes MC, Araújo LS, Souza LFGD, Jorge JCF (2016) Evaluation of the 625 nickel alloy weld overlays

deposited by electroslag process. Soldagem & Inspeção 21(4):417–427. https://doi.org/10.1590/0104-9224/si2104.03

27. Alvarães CP, Sandes SS, Jorge JCF, de Souza LFG, Araújo LS, Mendes MC, Dille J (2020) Microstructural characterization of Inconel 625 nickel-based alloy weld cladding obtained by electroslag welding process. J Mater Eng Perform 29:3004–3015. https://doi.org/10.1007/s11665-020-04861-3

28. Jorge JC, Meira OG, Madalena FCA, de Souza LFG, Araujo LS, Mendes MC (2017) Evaluation of the AISI 904L alloy weld over-lays obtained by GMAW and electro-slag welding processes. J Mater Eng Perform 26(5):2204–2212. https://doi.org/10.1007/s11665-017-2631-9

29. Falcón JCP, Echeverría A, Afonso CR, Carrullo JCZ, Borrás VA (2019) Microstructure assessment at high temperature in NiCoCrAlY overlay coating obtained by laser metal deposition. Journal of Materials Research and Technology 8(2):1761–1772. https://doi.org/10.1016/j.jmrt.2018.12.006

30. Xu X, Mi G, Chen L, Xiong L, Jiang P, Shao X, Wang C (2017) Research on microstructures and properties of Inconel 625 coatings obtained by laser cladding with wire. J Alloys Compd 715:362–373. https://doi.org/10.1016/j.jallcom.2017.04.252

31. Abioye TE, McCartney DG, Clare AT (2015) Laser cladding of Inconel 625 wire for corrosion protection. J Mater Process Technol 217:232–240. https://doi.org/10.1016/j.jmatprotec.2014.10.024

32. Tuominen J, Kaubisch M, Thieme S, Näkki J, Nowotny S, Vuoristo P (2019) Laser strip cladding for large area metal deposition. Additive Manufacturing 27:208–216. https://doi.org/10.1016/j.addma.2019.01.008

33. Hebbale AM, Srinath MS (2016) Microstructural investigation of Ni based cladding developed on austenitic SS-304 through micro-wave irradiation. Journal of materials research and technology 5(4):293–301. https://doi.org/10.1016/j.jmrt.2016.01.002

34. DuPont JN, Babu S, Liu S (2013) Welding of materials for energy applications. Metall Mater Trans A 44(7):3385–3410. https://doi.org/10.1007/s11661-013-1643-9

35. Iannuzzi M, Barnoush A, Johnsen R (2017) Materials and corrosion trends in offshore and subsea oil and gas production. npj. Materials Degradation 1(1):1–11. https://doi.org/10.1038/s41529-017-0003-4

36. Shamanian M, Kangazian J, Derakhshi MA, Szpunar JA (2019) Microstructure and mechanical properties of Inconel 617/AISI 310 electron beam welds. Metall Mater Trans A 50(7):3164–3173. https://doi.org/10.1007/s11661-019-05226-9

37. Araújo AD, Bastian FL, Castrodeza EM (2016) CTOD-R curves of the metal-clad interface of API X52 pipes cladded with an Inconel 625 alloy by welding overlay. Fatigue Fract Eng Mater Struct 39(12):1477–1487. https://doi.org/10.1111/ffe.12462

38. Silva CC, Miranda EC, Motta MF, Miranda HC, Farias JP (2012) Dilution control of weld overlay superalloys using taguchi method. In: 31st International Conference on Ocean, Offshore and Artic Engineering - OMAE2012, 2012, Rio de Janeiro. Proceedings of 31st International Conference on Ocean, Offshore and Artic Engineering - OMAE2012. New York: American Society of Mechanical Engineers ASME

39. CC Silva, CRM Afonso, AJ Ramirez, ÉM Miná, WM Aguiar, MF Motta, HC Miranda, JP Farias (n.d.) Microstructure and microchemistry of Hastelloy C276 dissimilar weld claddings. Metall and Mat Trans A [Submitted for publication].

40. Mannan MA, Golihue R, Kiser S, McCoy SA, Phillipp J (2016) A new nickel alloy filler metal designed for welding high strength ID-clad steels. In EUROCORR 50697:11–15

41. Silva RS, Miná EM, Dalpiaz G, Reppold RM, Paes MTP, Motta MF, Silva CC, Miranda HC (2020) Assessment of mechanical and metallurgical features of Inconel 680 weld metal. In: S. Tin et al.

(eds.), Superalloys. The Minerals, Metals & Materials Series. https://doi.org/10.1007/978-3-030-51834-9_42

42. ÉM Miná, G.M. Ferreira, R.S. Silva, R.M. Reppold, G. Dalpiaz, M.T. Piza Paes, M.F. Motta, H.C. Miranda, C.C. Silva (n.d.) Dissimilar girth welding of nickel-based alloy cladded pipelines: a new approach combining alloy 625 and low alloy steel as the filler metals for overmatch requirements. J. Mater. Proc. Tech. [Submitted for publication]

43. Lippold JC, Kiser SD, DuPont JN (2011) Welding metallurgy and weldability of nickel-base alloys. John Wiley & Sons

44. Wheeling RA, Lippold JC (2020) Weldability testing to understand composition effects on eutectic backfilling in Ni-30Cr alloys. Welding in the World 64(1):83–93. https://doi.org/10.1007/s40194-019-00806-0

45. Manikandan M, Arivazhagan N, Rao MN, Reddy GM (2015) Improvement of microstructure and mechanical behavior of gas tungsten arc weldments of alloy C-276 by current pulsing. Acta Metallurgica Sinica (English Letters) 28(2):208–215. https://doi.org/10.1007/s40195-014-0186-4

46. Goodwin GM (1987) Development of a new hot-cracking test–the sigmajig. Weld J 66(2):33s–38s

47. NIPPES, Ernest F.; SAVAGE, Warren F. (1949) Development of specimen simulating weld heat-affected zones. Weld J 28(11):534–546

48. Nakata K, Matsuda F (1995) Evaluations of ductility characteristics and cracking susceptibility of Al alloys during welding (materials, metallurgy & weldability). Transactions of JWRI, 24(1), 83-94. [53] KOU, Sindo. Solidification and liquation cracking issues in welding. Jom 55(6):37–42 2003

49. Kou S (2003) Library. In: Welding metallurgy. USA, New Jersey, pp 431–446. https://doi.org/10.1557/mrs2003.197

50. Savage, W. F. and Lundin, C. D. "The Varestraint Test," Welding Journal. October 1965 433-s to 442-s.

51. Savage, W. F. and Lundin, C. D., "Application of the Varestraint technique to the study of weldability," Welding Journal, November 1966 497-s to 503-s.

52. Senda T, Matsuda F, Takano G, Watanabe K, Kobayashi T, Matsuzaka T (1971) Fundamental investigations on solidification crack susceptibility for weld metals with Trans-Varestraint test. Trans Jpn Weld Soc 2(2):1–22

53. Arata Y, Matsuda F (1976) Solidification crack susceptibility of aluminum alloy weld metals (report I)—characteristics of ductility curves during solidification by means of the TransVarestraint test. Trans JWRI 5(21):53–67

54. Matsuda Y, Arata SK et al (1977) Solidification crack susceptibility in weld metals offully austenitic stainless steels (Report III)—effect of strain rate on cracking threshold in weld metal during solidification. Trans JWRI 6(21):197–207

55. Cieslak MJ, Headley TJ, Romig AD (1986) The welding metallurgy of HASTELLOY alloys C-4, C-22, and C-276. Metall Trans A 17(11):2035–2047. https://doi.org/10.1007/BF02645001

56. Rowe MD, Crook P, Hoback GL (2003) Weldability of a corrosion-resistant Ni-Cr-Mo-Cu alloy. WELDING JOURNAL-NEW YORK 82(11):313–31S

57. Santillana B, Boom R, Eskin D, Mizukami H, Hanao M, Kawamoto M (2012) High-temperature mechanical behavior and fracture analysis of a low-carbon steel related to cracking. Metall Mater Trans A 43(13):5048–5057. https://doi.org/10.1007/s11661-012-1331-1

58. Lippold J, Sowards J, Murray G, Alexandrov B, Ramirez A (2008) Weld solidification cracking in solid-solution strengthened Ni-base filler metals. In: Böllinghaus T, Herold H, Cross CE, Lippold JC (eds) Hot cracking phenomena in welds II. Springer, Berlin, Heidelberg. https://doi.org/10.1007/978-3-540-78628-3_9

59. JN D, BANOVIC SW, MARDER AR (2003) Microstructural evolution and weldability of dissimilar welds between a super austenitic stainless steel and nickel-based alloys. Weld J 82(6):125

60. Dupont JN (1996) Solidification of an alloy 625 weld overlay. Metall Mater Trans A 27(11):3612–3620

61. MJ CIESLAK et al (1988) A melting and solidification study of alloy 625. Metall Trans A 19(9):2319–2331

62. Dimitrios S et al (2019) Getting the strain under control: Trans-Varestraint tests for hot cracking susceptibility. Metall Mater Trans A 50(4):1748–1762

63. Jrnn D et al (1998) Solidification of Nb-bearing superalloys: Part I. Reaction sequences. Metall Mater Trans A 29(11):2785–2796